

Contemporaneous UV and Optical Observations of Direct and Raman Scattered O VI Lines in Symbiotic Stars

Jennifer J. Birriel

Department of Physics & Astronomy, University of Pittsburgh, Pittsburgh PA 15260;

jennifer@phyast.pitt.edu

Brian R. Espey

Space Telescope Science Institute, 3700 San Martin Drive, Baltimore MD, 21218;

espey@stsci.edu

Regina E. Schulte-Ladbeck

Department of Physics & Astronomy, University of Pittsburgh, Pittsburgh PA 15260;

rsl@phyast.pitt.edu

Received _____; accepted _____

ABSTRACT

Symbiotic stars are binary systems consisting of a hot star, typically a white dwarf, and a cool giant companion. The wind from the cool star is ionized by the radiation from the hot star, resulting in the characteristic combination of sharp nebular emission lines and stellar molecular absorption bands in the optical spectrum. Most of the emission lines are readily identifiable with common ions. However, two strong, broad emission lines at $\lambda\lambda 6825$ and 7082 defied identification with known atoms and ions. In 1989, Schmid made the case that these long unidentified emission lines resulted from the Raman scattering of the O VI resonance photons at $\lambda\lambda 1032, 1038$ by neutral hydrogen.

We present contemporaneous far-UV and optical observations of direct and Raman scattered O VI lines for nine symbiotic stars obtained with the Hopkins Ultraviolet Telescope (Astro-2) and various ground-based optical telescopes. The O VI emission lines are present in every instance in which the $\lambda\lambda 6825, 7082$ lines are present, in support of the Schmid Raman scattering model. We calculate the scattering efficiencies and discuss the results in terms of the Raman scattering model. Additionally, we measure the flux of the Fe II fluorescence line at $\lambda 1776$, which is excited by the O VI line at $\lambda 1032$, and calculate the first estimates of the conversion efficiencies for this process.

Subject headings: -atomic processes -binaries: symbiotic -ultraviolet: stars

1. INTRODUCTION

Roughly half of all known symbiotic stars exhibit two strong, broad emission lines at 6825 and 7082Å (Allen 1980). These emission features are much broader than other emission features ($\sim 20\text{Å}$) and are often among the ten strongest lines in the optical spectrum. These lines are only observed in symbiotic stars and, of those, only in systems that exhibit other high excitation features such as [Ne V] and [Fe VII]. For years the identity of these lines remained uncertain and they simply became known as the “unidentified” lines.

Schmid (1989) proposed that the long unidentified emission lines in the optical spectra of some symbiotic stars at 6825, 7082Å result from the Raman scattering of O VI resonance photons at 1032, 1038Å by neutral hydrogen. The Raman process involves the inelastic scattering of O VI photons produced near the hot component by neutral hydrogen atoms near the cool component of the binary system. An O VI photon excites a neutral hydrogen atom from the ground state to a virtual state between the $n=2$ and $n=3$ levels, followed by an immediate emission of a photon, which leaves the hydrogen atom in the excited $2s^2$ S-state. From energy conservation, the frequency of the scattered photon is the difference between the energy of the virtual and final states of the atom or, in wavelength terms: $\lambda_{\text{O VI}}^{-1} - \lambda_{\text{Ly}\alpha}^{-1} = \lambda_{\text{Raman}}^{-1}$. This change in energy by ~ 6.7 also results in a corresponding increase in the linewidth of the scattered lines, producing two broad lines in the red region of the spectrum (Nussbaumer, Schmid, & Vogel 1989).

Raman scattering is a dipole process which produces polarization. The Raman lines at 6825 and 7082 Å are generally observed to be strongly polarized, typically being 6% (Schmid 1996 and references therein). This strong polarization results because the scattering geometry in symbiotic systems is anisotropic. The O VI far-UV photons are produced near the hot star and Raman scattered near the cool star. Additionally, all the Raman photons are produced by a scattering process, so the polarization is not diluted by

light coming from an unscattered source. The strong polarization of the emission lines at 6825 and 7082 Å has been observed and extensively investigated in a number of symbiotics by several authors (Schmid & Schild 1994, 1997a,b, 2000; Harries & Howarth 1996a,b) and modeled in a number of papers (Schmid 1996, Harries & Howarth (1997), Lee & Lee 1997a,b).

Due to the small cross-section of Raman scattering, the main prerequisite for the production of the 6825, 7082Å emission is the presence of strong O VI emission. Indirect evidence of O VI emission in symbiotic systems includes the presence of O V λ 1371 emission that arises in part from dielectronic recombination from O VI (Hayes & Nussbaumer 1986), and the presence of Fe II transitions which are excited by O VI photons (Johansson 1988; Fiebelman, Bruhweiler, & Johansson 1991). Far-UV observations of a few symbiotic stars using *Voyager* found strong evidence for Ly β /O VI emission (Li & Leahy 1997), however, the low resolution, ~ 20 Å, made it difficult to determine the exact amount of O VI and Ly β present in each object. In 1993 the ORFEUS-I mission made unambiguous detections of O VI in a small number of symbiotic stars (Schmid et al. 1999) and, during the flight of the Astro-2 in 1995, Espey et al. (1995) used far-UV data from the Hopkins Ultraviolet Telescope or HUT and optical data from the Anglo-Australian Telescope (AAT) to provide the first simultaneous observations of both the O VI 1032, 1038 Å and scattered 6825, 7082 Å lines in the symbiotic star RR Tel. More recently, Birriel et al. (1998) used far-UV data from the HUT and near-simultaneous optical data to determine the Raman scattering efficiency in the symbiotic star Z And. Schmid et al. (1999) presented far-UV observations from ORFEUS-I and II showing strong O VI emission for six symbiotic stars and used available, though not necessarily contemporaneous, optical observations to determine scattering efficiencies for the Raman process.

In this paper we examine contemporaneous ultraviolet and optical observations for

nine symbiotic stars taken with the HUT (Astro-2) and various ground-based optical telescopes. In support of the Schmid Raman scattering hypothesis, we find no case in which the 6825, 7082 Å lines appear in the optical without the O VI 1032, 1038Å emission simultaneously occurring in the far-UV spectral region. We calculate scattering efficiencies where possible, compare these to the results of Schmid et al. (1998) and discuss possible scattering geometries. In addition, we make the first determinations of the efficiency for the Bowen fluorescence process in which a O VI 1032 Å photon excites the Fe II 1776.5 Å line (actually an unresolvable blend of the 1776.660 Å and 1776.418 Å lines).

2. OBSERVATIONS

Far-UV data from the HUT were obtained during the Astro-2 mission in March 1995 (see Table 1). HUT data cover the wavelength range of 825-1850Å with a nominal resolution of ≈ 3 Å. A detailed description of the HUT and its calibration and performance during the Astro-2 mission can be found in Davidsen et al. (1992) and Kruk et al. (1995), respectively. Kruk et al. (1999) provide a description of the acquisition of the ultraviolet spectrum of each object. Espey et al. (1995) describe the data processing for HUT spectra.

The HUT spectra used in this study are listed in Table 1a. We list relevant details for each observation including acquisition date, exposure time, slit diameter, and photometric corrections. The HUT symbiotic spectra were obtained during orbital day and hence contain strong airglow emission lines. In some observations, pointing errors resulted in flux loss. The HUT team determined photometric correction factors to account for these losses and the final calibrated spectra for most symbiotic stars have flux accuracies of $\sim 5\%$ (Kruk et al. 1999). During the observation of CH Cyg the measured flux varied gradually, rising and falling by almost 50%. The pointing was fairly stable and the flux variations were not correlated with any changes in pointing, thus the photometric correction listed in Table 1

is probably not meaningful. For most objects, the signal-to-noise in the continuum region near the O VI emission is ~ 10 per pixel ($\sim 0.51\text{\AA}$).

Many of the optical observations for this study were taken around the time of the Astro-2 mission by Mikołajewska & Kenyon (see Table 1b). The data were obtained using the FAST spectrograph mounted on the 1.5-m telescope at the Fred L. Whipple Observatory on Mount Hopkins, AZ. These data cover a spectral range 3800-7500 \AA at a resolution of $\sim 3\text{ \AA}$. The symbiotic spectra were calibrated using FAST spectra of several Hayes & Latham (1975) flux standards.

Some of the optical observations on 3 Jan 1995 and 3 April 1995 were affected by the presence of thin clouds which resulted in inaccurate spectrophotometry. We used a synthetic photometry program written by one of us (BRE) to estimate the scalar correction required to bring the derived photometry into agreement with the broad-band photometry of Hric et al. (1996a; 1996b). The applied photometric scale factor is indicated in Table 1b. For Z And and CH Cyg, both of which have very good photometric coverage, agreement between observed and synthetic photometry (using B, V, and sometimes R magnitudes) is better than 10%, giving us confidence in our synthetic photometry estimates. For EG And, the photometric coverage is sparse, but brackets the time of observation. Amateur observations by the Association Française d’Etoiles Variables (available on the web at <ftp://cdsarc.u-strasbg.fr/pub/afoev/>) were used to estimate the variation between the photometric data. For AG Dra and AX Per, on the other hand, very good coverage exists, with photometric observations within a week or two of the ground-based data. Simple linear interpolation was used to estimate the fluxes at the time the spectroscopic data were taken. In view of the calibration required for these data, flux errors of $\approx 20\%$ are probably a reasonable assumption. We compared our recalibrated spectra with others obtained close in time (or phase) to these observations and found that continuum and emission line fluxes

agree to within $\sim 20\%$.

Contemporaneous optical observations are not available for HM Sge. Schmid & Schild obtained an optical spectrum of HM Sge on the night of 15 July 1995 with the 4.2-m telescope of the Royal Greenwich Observatory on La Palma, Canary Islands. The spectral resolution was 0.65 \AA . The emission at $\lambda\lambda 6825, 7082$ is very weak, and the data are not fluxed, thus we cannot derive an estimate for the scattering efficiency. Lower resolution spectra obtained using the WIYN telescope nearly a year later also show a very weak feature in the region of $\lambda 6825 \text{ \AA}$ while the emission feature at $\lambda 7082 \text{ \AA}$ is not visible.

3. ANALYSIS

The data were measured using the SPECFIT χ^2 -minimization routine (Kriss 1994) running under the IRAF¹ data reduction package. SPECFIT has the advantage that a variety of functional forms can be used to describe the continuum, emission lines, and absorption lines. Additionally, user-defined functions can be used to model the absorption features and airglow emission lines. Observed fluxes for the O VI lines were measured assuming a simple linear fit to the continuum and Gaussian profiles for the $1032, 1038 \text{ \AA}$ lines. At the modest resolution of the HUT, ($\sim 3 \text{ \AA}$ at the O VI doublet), the O VI lines are partially blended and the linewidths unresolved (see Figure 1). To measure the O VI components, we tied the ratio of the emission line wavelengths at the theoretical value (Morton 1991) and the width of the weaker line was tied to that of the stronger line.

¹The Image Reduction and Analysis Facility (IRAF) is distributed by the National Optical Astronomy Observatories, which is operated by the Association of Universities for Research in Astronomy, Inc. (AURA) under cooperative agreement with the National Science Foundation.

Observed fluxes for the optical lines at 6825, 7082 Å were measured using a similar approach. However, the fit to the continuum depended on the spectral type of the cool red giant star. For objects with a K-type giant star, such as AG Dra, V1016 Cyg, HM Sge, and RR Tel, the continuum was modelled with a simple linear fit in the region near the emission features. The 6825, 7082Å emission lines were fitted with Gaussian profiles. In the case of Z And, EG And, BF Cyg, CH Cyg, and AX Per the optical continuum is that of a M-type giant star. Kenyon & Fernandez-Castro (1987) examined the depth of TiO and VO absorption bands in the red spectra of symbiotics and concluded that most symbiotic stars contain normal red giants. We used SPECFIT to find the best-fit spectra from the observed sample of Fluks et al. (1994) to the optical continua of the Z And, EG And, BF Cyg, CH Cyg, and AX Per. Table 5 shows our derived optical spectral types for these objects and compares them to the results of Kenyon & Fernandez-Castro. The spectral type of the red giant probably depends on illumination effects and so we give the orbital phase of the optical observations used here; Kenyon & Fernandez-Castro give spectral types based on spectra obtained near the photometric minimum for each object. The 6825, 7082Å lines were represented by Gaussians which were tied together by width and by their rest wavelength ratio.

Table 2 gives the observed fluxes of both the direct and Raman scattered O VI lines. In general the UV line fluxes are good to 10% or better and the optical line fluxes to 20% or better. The HUT far-UV spectra and the optical spectra are presented in Figures 1–3.

3.1. Interstellar H₂ Absorption in the O VI Line Region

For comparison with other authors, we list in Table 2 the observed fluxes of the O VI lines as measured relative to a local linear continuum in the HUT spectra. We expect the ratio of the O VI 1032Å and the 1038Å lines to be somewhere between the optically thin

(2:1) and thick (1:1) values, but a quick glance at Table 2 shows that the observed ratios for Z And, V1016 Cyg, and AG Dra exceed the optically thin value of 2:1. Schmid et al. (1999) also find that the observed O VI flux ratios exceed the optically thin ratio; in addition, their observed ratios are rather different than those found in this study. The discrepancies between the HUT and ORFEUS data may be due to variations in the O VI line fluxes; this is discussed further in §3.4.

We attribute these anomalously high ($f(1032)/f(1038) > 2.0$) O VI flux ratios for Z And, V1016 Cyg, and AG Dra, to attenuation by interstellar absorption. The far-ultraviolet wavelength region where the O VI emission lies is subject to significant absorption due to interstellar atoms and molecules, in particular H₂. The 1032 Å line is relatively uncontaminated, whereas the line at 1038 Å sits in a strong absorption band (Morton 1975). In the HUT data for Z And and V1016 Cyg we see absorption features attributable to H₂ at wavelengths below 1130 Å, though these features are not quite as evident in the spectrum of AG Dra. The spectra of CH Cyg and RR Tel show only weak, if any, absorption as these objects are located high above the Galactic plane.

Determination of scattering efficiencies for both the 1032 Å and 1038 Å lines requires that we know the actual fluxes emitted within the region near the hot star, before any extinction and/or absorption due to interstellar dust and gas. Hence we must account for interstellar H I and H₂ absorption in order to determine the scattering efficiencies for the Raman process in Z And, V1016 Cyg, and AG Dra. A fit to the UV continuum of each object allows us to estimate the amount of absorption due to these species. We can then perform a simple calculation to correct the emission line fluxes for H₂ absorption.

3.2. UV Continuum Fits

Two sources contribute to the ultraviolet continuum in the HUT spectral region: the hot star and the nebula. We use a simple blackbody spectrum for the hot star and model the nebular contribution assuming that the dominant source is H I Balmer recombination radiation. The resultant continuum is attenuated using the extinction curve of Cardelli, Clayton and Mathis (1989, hereafter CCM). For continuum fitting we choose regions free of both emission and absorption line features.

The free parameters for the fitting procedure are the blackbody temperature, the flux emitted by the hot star at 5500 Å, the electron temperature of the nebula, the flux at the Balmer edge (3646 Å), and the extinction. The flux emitted by the hot star is a function of the hot star temperature, the stellar radius, and the star’s distance; likewise, the flux emitted by the nebula is a function of the nebular electron temperature, nebular size, etc. In order to reduce the number of free parameters, and thus the complexity of the fitting procedure, we fix the values of the hot star temperature and the nebular electron temperature. We applied the modified Zanstra method of Mürset et al. (1991) together with the equivalent width of the He II 1640 Å line to determine the hot star temperature. In Table 3 we compare our derived values with those of Mürset et al. For AG Dra and CH Cyg, our derived temperatures are much lower than found by Mürset et al. We use their value because our observations of AG Dra and CH Cyg were obtained during outburst (Tomova & Tomov 1999, González-Riestra et al. 1999, Greiner et al. 1997; Espey et al. 1995b, Munari et al. 1996). The modified Zanstra method is not valid during outburst as the enhancement in the continuum is greater than that in the He II line, and the continuum shape changes rapidly during outburst; this problem is discussed in greater detail in Mürset et al. (1991). Additionally, Mikołajewska et al. (1995) point out that the intensities of various high ionization lines such as He II and N V require a hot star temperature in excess

of 10^5 K. In modeling the nebular recombination continuum radiation, we must specify the electron temperature, typically $\sim 1.5 \times 10^4$ K; here we chose values found in the literature (Mikołajewska & Kenyon 1996, Mikołajewska et al. 1995, and Nussbaumer & Schild 1981).

The spectrum below 1130 Å is affected by the presence of interstellar H I and H₂. We fit the absorption lines by scaling a template consisting of optical depth *vs.* wavelength. Our template is derived from recent theoretical data of H₂ rotational transitions of Abgrall et al. (1993a, b), broadened to a FWHM of 5 km s⁻¹ which is typical of cool interstellar gas (Morton 1975, van Dishoeck & Black 1986 and references therein). The relative scaling of the optical depths comes from the observed interstellar H₂ column densities obtained from ORFEUS-II observations of Galactic stars (Dixon et al. 1998). The resulting theoretical model is convolved with the instrumental resolution (Kruk et al. 1998), before fitting to spectral regions affected solely by H₂. Once the overall H₂ column density is obtained, its contribution is fixed, and absorption due to H I is determined by fitting the spectral regions affected by its influence alone.

We successfully fit the HUT UV continua of Z And, EG And, BF Cyg, V1016 Cyg, AG Dra, and AX Per and the derived extinction values for these objects are found in Table 4. The fit to the UV-spectra in the O VI line region is displayed in figures 1-3 as a dotted line overplotted on the HUT data. We did not fit the HUT UV continuum of RR Tel as described above; its observed line ratio does not indicate significant H₂ absorption and there are no observable H₂ absorption bands in its far-UV spectral region. We were unable to obtain continuum fits for the HUT spectra of HM Sge and CH Cyg. The continuum of HM Sge is too flat and too weak in the far-UV region to allow for fitting. Above 1200Å the HUT UV spectrum of CH Cyg shows P-Cygni absorption features and a continuum shape typical for late A-type supergiants and we therefore do not fit this object's continuum with our hot star-nebular continuum model.

We are mostly concerned with those objects which exhibit the Raman scattering effect, i.e. those objects with both the O VI in the far-UV and the emission at 6825Å and 7082Å. Our best fits to the continua of Z And, V1016 Cyg, and AG Dra are found in Table 6; here we list the derived parameters of extinction, H I column density, and H₂ column density and the values of the adopted hot star temperature and nebular electron temperature. The continuum fits for the region below 1130Å are illustrated in Figure 4; these fits consist of a blackbody spectrum reddened by the CCM (1989) extinction curve and include interstellar H I and H₂ absorptions and terrestrial N I, O I, and Ly β airglow.

3.3. O VI Emission Lines and H₂ Absorption Corrections

Our method of correcting for unresolved molecular hydrogen absorption will not work for emission lines. In the emission line case, the discrete nature of the emission lines, and their finite width relative to the absorption, precludes direct estimation of the contamination from their unresolved profiles. Correcting the O VI emission lines for molecular absorption requires a number of steps and follows the approach discussed in Birriel, Espey, and Schulte-Ladbeck (1998). The absorbed O VI line strength is measured using the absorbed continuum discussed in Section 3.3, next a correction factor is determined, then the final line flux is obtained by correcting the flux for the presence of molecular hydrogen lines.

The H₂ template is generated at 0.01 Å resolution with column density set to the values used for the continuum fit (Table 6). The emission lines are modeled as Gaussians with intrinsic widths of ~ 70 km/s based on the preliminary estimates from Orfeus-I and -II data (Schmid et al. 1999). It is most likely that the relative velocity of any molecular cloud and the emitting symbiotic will be non-zero; since the cloud lies somewhere between the earth and the symbiotic, we expect that its velocity will be somewhere between that of the sun and the symbiotic star. We assume the relative velocity of the absorption and

emission components to be about half the heliocentric radial velocity of the symbiotic system. Heliocentric radial velocities for Z And, V1016 Cyg, and AG Dra are taken from the high-resolution echelle spectra of Ivison, Bode, & Meaburn (1994). The amount of absorption of each far-UV emission line is estimated by integrating the product of the emission and absorption line profiles across each emission line. In general, the $\lambda 1032$ line suffers only slight absorption ($\sim 10\%$) while the flux in $\lambda 1038$ line is significantly reduced.

Table 7 lists the transmission factors which have also been incorporated into the corrected O VI flux values shown in Table 8. The corrections for H₂ made in this study assume a single cloud along the line of sight and thus do not account for multiple cloud absorptions or circumstellar absorption. The revised flux ratios for Z And, V1016 Cyg, and AG Dra are closer to the optically thin ratio (2:1), see Table 8. We point out that under the Raman scattering model of Schmid (1996) the in-situ relative flux emitted by the gas can be altered by subsequent passage through the scattering medium. Because of the larger Rayleigh scattering and photon-destruction cross-sections, the $\lambda 1032$ line photons undergo much more interaction. Thus, the simple 2:1 flux ratio which is expected under nebular conditions can actually be somewhat higher or lower than 2, depending on phase angle. In particular Schmid finds $f(1032)/f(1038) < 2$ for phase angles where absorption is important and > 2 for phase angles where the reflection effect is significant.

3.4. O VI Line Flux Variations

In symbiotic stars, emission line fluxes vary on time scales from as little as a few weeks to as long as years. These variations are the result periodic obscuration due to the binary orbit or of outburst activity of the hot star. Many of the same symbiotic systems were observed using the HUT (Astro-2) and ORFEUS-I and -II instruments in March 1995, September 1993, and November 1996, respectively. In order to assure consistency with

Schmid et al. (1999) we will compare the fluxes of the O VI lines from the HUT data measured relative to the local linear continuum in the O VI region. For the discussion that follows we are careful to adopt Orfeus-I and -II fluxes from measurements which are free of losses due to saturation or misplacement of the target in the aperture (Schmid et al. 1999). If we compare the spectra from 1993 to 1996, we see clear variations in the O VI line fluxes for Z And, AG Dra, V1016 Cyg, and RR Tel, see Table 9. In AG Dra, the 1032Å line flux decreases steadily from 1993 to 1996; the 1038Å flux decreases by almost 50% from 1993 to 1995 but does not appear to change significantly from 1995 to 1996. In the case of Z And, the 1032Å line flux remains relatively constant from 1993 to 1995 but increases by $\sim 40\%$ from 1995 to 1996 while the 1038Å line flux increases by $\sim 70\%$ from 1993 to 1995 and remains unchanged from 1995 to 1996. For RR Tel, the fluxes of both O VI lines decreased slightly over the period from 1993 to 1996. In V1016 Cyg, the flux of the 1032Å line remained constant from 1995 to 1996, while the 1038Å line flux doubled.

Given the differences in both resolution and signal-to-noise between the HUT and the ORFEUS-I and -II instruments, it is natural to wonder if these variations in flux are real. In each study, the observed O VI line fluxes are measured relative to the local linear continuum on either side of the O VI emission (Schmid et al. 1999). The continuum in each object is so weak relative to the O VI emission that differences in the choice of the continuum level and the signal-to-noise in the continuum are not particularly critical for the determination of the O VI line fluxes. The higher resolution ORFEUS data show no lines in the vicinity of the O VI emission which could be blended with the O VI lines, and hence unresolved, in the lower resolution HUT data. Thus, we believe that the observed flux variations between the HUT and ORFEUS data are real and not an artifact of either differences in instrumental properties or analysis technique.

In principle, the observed O VI line fluxes can vary for a number of reasons. Many

symbiotic stars show variations in emission line fluxes with orbital phase (Kenyon 1986) and these variations are associated with the binary nature of the systems. Part or all of the line emitting portion of the ionized nebula surrounding the hot star can be completely occulted by the red giant, resulting in decreased emission line fluxes. Additionally, Shore & Aufdenberg (1993) have shown that the outer atmosphere of the red giant star can effectively absorb flux from many emission lines; such “atmospheric eclipses” would also result in flux variations in observed emission lines over the course of the binary orbital period. In the models of Schmid (1996) the simple O VI flux ratio (2:1 under optically thin conditions) is sensitive to the orbital phase of the system. The $\lambda 1032$ line photons undergo much more interaction in the H^0 region than the $\lambda 1038$ line photons; this is due to the fact that the shorter wavelength photons have a 5.2 times larger Rayleigh scattering cross-section and a 2.3 times greater photon-destruction cross-section. Thus, depending on the orbital phase, the flux ratio $f(1032)/f(1038)$ can sometimes be either less or greater than 2. This is the most likely explanation for the variations in the observed flux ratios for Z And, V1016 Cyg, and AG Dra. Outburst activity also results in changes in emission line fluxes as well as continuum emission (Kenyon 1986): many emission lines weaken considerably as the brightness increases during an outburst and strengthen as the brightness fades.

The decreasing flux in both O VI lines of RR Tel is consistent with the slow evolution of the RR Tel spectrum which has been observed over a number of years (Nussbaumer & Dumm 1997, Contini & Formigini 1999); but, the source of flux variations in the other three objects is more complicated. The UV emission lines of O VI and N V should show similar flux variations with orbital phase because they have similar properties: both are resonance doublets of highly ionized species and both have wavelengths close to a Lyman transition where the Rayleigh scattering cross-sections are large (Schmid 1995, 1996; Schmid et al. 1999). The N V 1240\AA line in Z And varies markedly with orbital phase

(Fernández-Castro et al. 1988, 1995). In AG Dra, the N V 1240Å line also shows significant variations with orbital phase (Mikołajewska et al. 1995, González-Riestra et al. 1999). The HUT observations in March 1995 were obtained after outburst activity from June to November 1994 and before a secondary outburst which began in July 1995. The Orfeus-II observations in 1996 were obtained near the end of an outburst. The variations in observed O VI line flux in AG Dra from 1993 to 1996 are probably the result of both outburst activity and orbital variation. On the other hand, Z And was in quiescent state from 1988 to 1997 and V1016 Cyg has been in quiescence since about 1985, so it would seem that the variations in O VI line fluxes are the result of orbital motion in these systems.

4. Raman Scattered O VI Lines

Raman scattering of O VI photons can occur only in high-excitation symbiotic systems where O^{+5} ions exist. To give rise to Raman scattered emission, a high-excitation source is required to produce the O VI photons, and a large H I column is necessary in order to provide the scattering source. Of the total sample of high excitation systems examined to date, roughly 70% exhibit the Raman scattered features at 6825, 7082 Å (Schmid 1992). Of the six systems in our study that have O VI 1032, 1038 Å emission, four (Z And, V1016 Cyg, AG Dra, and RR Tel) exhibit Raman-scattered O VI emission, one (HM Sge) shows occasional evidence for the scattered lines, and one (CH Cyg) has never been seen to exhibit the scattered features. The statistics of our (admittedly small) sample are therefore consistent with Schmid’s results (1992).

As mentioned previously, no simultaneous optical observations of HM Sge were available for comparison with the HUT far-UV data. Schmid et al. (2000) report that the Raman features have only recently emerged in the optical spectrum of HM Sge. Their optical spectrum from July 1995 shows weak emission features at $\lambda\lambda$ 6825,

7082. The data are not fluxed but the measured relative strengths of the Raman lines $EW(6825)=(4.6\pm 0.3)\times EW(7082)$ are consistent with the results of Allen (1980). A lower resolution observation of HM Sge taken over a year later with the WIYN is fluxed, see Table 2; the $\lambda 6825$ feature is again weak and the $\lambda 7082$ feature is not visible. The variation in HM Sge photometry (<ftp://cdsarc.u-strasbg.fr/pub/afoev/>) for Astro-2/La Palma/WIYN observations quoted as a flux ratio is 1.00/0.97/1.03. We take the continuum flux of the WIYN observations to be the same as the La Palma observation, consistent with the photometry. The observed flux during the La Palma observation is thus 1.4×10^{-14} erg cm⁻² S⁻¹. Taking $E(B-V)=0.65$, 0.40 the estimated scattering efficiencies are 0.5 to 0.7%, respectively. As HM Sge is one of the hottest white dwarf symbiotic systems, this is consistent with the picture requiring a high density region of H I. In the case of HM Sge, the H I is probably nearly totally ionized. Schmid et al. (2000) explain the sudden appearance of the Raman lines by a strong decrease of the absorption of the far-UV emission lines at Ly β and O VI by dust associated with the system itself. This implies that further correction to the Raman scattering efficiency factor might be necessary.

CH Cyg also exhibits strong O VI emission but no Raman features and, to our knowledge, has never exhibited the Raman lines. A WIYN spectropolarimetry observation taken on 9 April 1996 shows a strong polarization variation in H α , but no polarization in excess of the continuum polarization in the regions of the Raman lines. In addition, CH Cyg has been monitored at the Pine Bluff Observatory (<http://www.sal.wisc.edu/HPOL>) for a number of years and neither Raman line has been observed either in the flux or polarization spectra. The models of Schmid (1996) and Harries & Howarth (1997) indicate that the bulk of the Raman scattered photons are produced in the region between the hot and cool components of the symbiotic system. Thus, in order for the Raman scattering process to be effective, the region between the two stars must contain a high density of H⁰ scatterers. CH Cyg shows P-Cygni features indicating an extensive outflow of gas and has undergone

several outbursts since 1965 (Mikołajewska, Mikołajewska, and Khudyakova, 1990; Skopal et al. 1996). Why then does CH Cyg not exhibit the Raman features in the optical? Munari et al. (1996) identified several episodes of dust condensation in the wind of the red giant and one of these occurred during the period spanning 1995 and 1996. According to Munari et al. the spectroscopic and photometric observations of CH Cyg suggest that the dust condensation occurs in a spherically symmetric wind around the red giant star and that the white dwarf star lies well outside the dust. We suggest then that the absence of the Raman features in CH Cyg is, like the case of HM Sge, due to the absorption of the far-UV O VI photons by circumstellar dust in or near the neutral scattering region. Interestingly, CH Cyg is an S-type symbiotic system whereas HM Sge is a D-type system so it seems that the suppression of the Raman effect by circumstellar dust is not limited to the D-type systems.

4.1. Extinction Re-examined

The extinction values for symbiotic stars are notoriously difficult to derive. Many of the extinction values obtained from our fits to the HUT UV data are quite different from the values derived by previous authors using a variety of methods. Since the accuracy of the scattering efficiencies depends sensitively on the extinction correction, we feel that it is appropriate to re-examine extinction values at this point. Table 4 summarizes the extinction estimates of other researchers and those derived in this study. The extinction values adopted for use in line flux corrections for objects which exhibit the Raman scattering effect are indicated in bold in the table.

As noted in §4, data for both CH Cyg and HM Sge are consistent with the presence of dust in or around the symbiotic system. To derive extinction estimates appropriate to the O VI lines, then, it is necessary to choose a diagnostic arising from material within the

same gas. Emission lines provide easily measured features and lines from He II and [Ne V] are good candidates. As the O VI region is also likely to be concentrated around the hot star, stellar continuum fits provide an alternative measurement technique.

As a starting point, we assume Case B conditions and utilize the He II line ratios to determine extinctions for each object. Proga et al. (1996) point out that illumination effects in symbiotics can result in significant deviations from Case B conditions, making the He II line ratios poor reddening diagnostics unless the hot star luminosity and temperature are well known. Nonetheless, we believe that the He II line ratios can still be used as an effective indicator of reddening if the results derived from the three line ratios 1085/1640, 1085/4684, 1640/4686 are consistent with their case B values. We derive extinctions by comparing the observed He II line ratios to the theoretical Case B line ratios of Storey & Hummer (1995). We assume that the emitting gas is optically thin. For individual objects we assume nebular conditions as follows: Z And, $T_e \sim 20,000$ K, $N_e \sim 10^9$ cm $^{-3}$ (Birriel, Espey, Schulte-Ladbeck 1998); V1016 Cyg $T_e \sim 20,000$ K, $N_e \sim 10^7$ – 10^8 cm $^{-3}$ (Nussbaumer & Vogel 1990); AG Dra $T_e \sim 15,000$ K, $N_e \sim 10^9$ – 10^{10} cm $^{-3}$ (Mikołajewska & Kenyon 1992); RR Tel $T_e \sim 20,000$ K, $N_e \sim 10^6$ cm $^{-3}$ (Espey et al. 1995a). In Z And and V1016 Cyg, the three He II line ratios yield consistent reddening values and we conclude that the assumption of Case B conditions is valid for these objects. On the other hand, the derived reddening for RR Tel and AG Dra varies considerably depending on which He II line ratio is used (Table 4). The He II 1085 line suffers only nominal absorption (less than 5%) from interstellar H $_2$, and thus absorption cannot explain the discrepancies among the derived reddening values. Our conclusion is that the nebular gas of both AG Dra and RR Tel departs from simple Case B conditions.

Schlegel, Finkbeiner, and Davis 1998 (hereafter SFD) have recently constructed a full-sky map of the Galactic dust. Their map is a reprocessed composite of the *COBE*/DIRBE

and *IRAS/ISSA* maps and has a resolution of $6''.1$ and are shown to predict reddening with an accuracy of 16%. The new dust map leads to reddening estimates which are consistent with the Burstein-Heiles maps in most regions of the sky but are twice as accurate and appear to be much more reliable in regions of high extinction (SFD). The authors have made the map and software for deriving extinctions readily available for general use. In Table 4, we have listed the extinctions based on this new dust map for each of our nine symbiotic stars.

For each object, with the exceptions of CH Cyg and HM Sge, we obtain an extinction value from our fitting of the HUT UV continuum. A quick perusal of Table 4 shows that the extinction values derived from a fit to the HUT UV continuum are generally rather different from the values obtained by previous fits to the IUE UV continuum (Mürset et al. 1991) and other methods. Our fits to the HUT continuum assume the extinction curve of Cardelli, Clayton, and Matthis (1989) while Mürset et al. assume the extinction curve of Seaton. These two extinction parameterizations differ significantly for $\lambda < 1500\text{\AA}$. In addition, Mürset et al. fit the IUE spectra by eye and apply no reasonable numerical criterion for the quality of the fit whereas our results are based on a χ^2 -minimization technique. The differences between our derived extinction values and those of Mürset et al. are most likely a combination of the above mentioned differences in fitting technique. However, the results of our continuum fitting generally agree well the extinction values derived from the dust maps of SFD. The results of our continuum fits for AG Dra, 0.08 ± 0.01 , and RR Tel, 0.08 ± 0.02 , respectively, are in good agreement with previous studies as well as with the recent results of SFD.

In the case of Z And, we derive an extinction of 0.21 ± 0.01 from our continuum fit and 0.24 ± 0.03 taking the theoretical Case B He II line ratios from Storey and Hummer (1995). While these values are consistent with one another, they are slightly lower than the

values generally adopted by other groups (Table 4). Mikołajewska & Kenyon (1996) give a thorough discussion on the various determinations of the extinction for Z And. Since our results are also in agreement with the extinction estimates from the recent results of SFD, we assume an extinction of 0.24 ± 0.03 for Z And as derived from our He II ratios.

Previous estimates for the reddening of V1016 Cyg range from 0.20 ± 0.10 to 0.30 ± 0.10 , see Table 4. We derive 0.24 ± 0.03 from our fit to its HUT UV continuum. Assuming Case B recombination conditions (Storey & Hummer 1995), the He II line ratios $1640\text{\AA}/4686\text{\AA}$ and $1085\text{\AA}/4686\text{\AA}$ yield a reddening of 0.35 ± 0.04 . Using the dust maps of SFD, the reddening in the direction of V1016 Cyg is 0.25 ± 0.04 . We adopt the extinction derived from our continuum fit for V1016 Cyg, $E(B-V) = 0.24 \pm 0.03$, as this is more consistent with the SFD results than the higher results derived using the He II ratios.

4.2. Raman Scattering Efficiencies

The Raman scattering efficiency is defined as the photon ratio of the Raman scattered line and the initial O VI line component, $N_{\text{Raman}}/N_{\text{O VI}}$, i.e. the fraction of emitted O VI photons converted to Raman photons. From the ratios of the dereddened fluxes, $F_{\lambda 6825}/F_{\lambda 1032}$ and $F_{\lambda 7082}/F_{\lambda 1038}$, we derive the photon ratios and hence the scattering efficiencies for each O VI line (see Table 10). The uncertainties in the conversion efficiencies are dominated by the uncertainties in the extinction values. RR Tel and AG Dra have fairly well determined extinctions and thus their derived scattering efficiencies are relatively accurate. For RR Tel, V1016 Cyg, and Z And, the conversion efficiency for the $\lambda 1032 \rightarrow \lambda 6825$ process is higher than the $\lambda 1038 \rightarrow \lambda 7082$, as a result of the larger scattering cross section for the former process relative to the latter. In the case of AG Dra, the scattering efficiencies are very similar. This is in qualitative agreement with Schmid et al. (1999), whose contemporaneous far-UV and optical data for AG Dra in 1995 also yielded a similar

scattering efficiency for both the 1032 Å and 1038 Å line photons. Given the difference in orbital phases for the AG Dra observations in this study and those of Schmid et al., it is difficult to explain the similarity of the two Raman processes as a result of orbital effects (Schmid 1996). One possible explanation is that the circumstellar material in the AG Dra system is such that a 1032Å photon is absorbed or scattered much more than a 1038Å photon, resulting apparently similar scattering efficiencies for both processes.

Our scattering efficiencies for the Raman process in RR Tel and Z And agree well with those of Schmid et al. (1999) while our results for V1016 Cyg and AG Dra are quite different. For V1016 Cyg our scattering efficiency is ~ 2 times larger for the $\lambda 1032 \rightarrow \lambda 6825$ process and ~ 3 times larger for the $\lambda 1038 \rightarrow \lambda 7082$ process. In the case of AG Dra, our derived efficiencies for both Raman processes are ~ 3 times smaller than those determined by Schmid et al., though the similarity in scattering efficiency for both O VI doublet lines is consistent with their findings. For V1016 Cyg and AG Dra, our derived scattering efficiencies differ from those of Schmid et al. through our adoption of a different extinction estimate for each object and our use of optical spectra contemporaneous with our far-UV data.

The derived scattering efficiencies can be compared to the models of Schmid (1996). For the discussion that follows, we assume the “basic” model: in this model the photons are initially released as far-UV O VI line photons from an extended emission region in the ionized nebula and may undergo multiple scatterings before escaping. The scattering efficiency depends strongly on the ionization geometry as described by the X_{H^+} -parameter defined by Seaquist et al. (1984). The dimensionless X_{H^+} -parameter is related to the ionizing photon luminosity of the hot source L_H , the binary separation p , and the wind parameters of the cool giant (\dot{M}, v_∞) according to

$$X_{H^+} \sim pL_H \left(\frac{v_\infty}{\dot{M}} \right)^2.$$

The scattering efficiencies for RR Tel and Z And suggest that about one in every three emitted O VI photons interacts with the scattering region either via Raman scattering, Rayleigh scattering or absorption. The inferred scattering geometry is a cone-shaped neutral hydrogen region around the cool giant which is irradiated by an extensive O VI emitting region surrounding the hot star, somewhere between the X_{B3} and X_{C3} models of Schmid (i.e. X_{H+} between 4.0 and 0.4). For V1016 Cyg and AG Dra, which exhibit similar scattering efficiencies, about 50% (or roughly one in two) of the emitted O VI photons interact with the scattering region. For V1016 Cyg and AG Dra the suggested scattering geometry appears to be quite close to the X_{C3} model of Schmid, i.e. a large neutral hydrogen region irradiated by a much more confined O VI emission zone surrounding the hot star (i.e. $X_{H+} \sim 0.4$). The X_{H+} parameters derived here are in qualitative agreement with the results of Mürset et al. (1991) in that $0.3 \leq X_{H+} \leq 4$ for these four symbiotic systems. However, the Raman scattering efficiency for V1016 Cyg implies that X_{H+} is very close to 0.4 whereas Mürset et al. derive a much larger value of $X_{H+} \sim 2.3\text{--}3.7$.

The models of Schmid (1996) and Harries & Howarth (1997) show that, as expected, the production of Raman-scattered O VI photons is increased for more extended and dense neutral scattering regions. Speaking quite generally, our derived Raman efficiencies imply that V1016 Cyg and AG Dra have higher mass loss rates than Z And and RR Tel. Using Figure 12 of Schmid (1996), the derived efficiencies for AG Dra and V1016 Cyg yield a mass loss rate of $\sim 3 \times 10^{-6} M_{\odot}$ and for Z And and RR Tel $\sim 1 \times 10^{-6} M_{\odot}$. From radio measurements at 3.6 cm, Seaquist, Krogulec, & Taylor (1993) report mass loss rates of $1.3 \times 10^{-5} M_{\odot}$ for V1016 Cyg, $6.3 \times 10^{-6} M_{\odot}$ for RR Tel, $1.8 \times 10^{-6} M_{\odot}$ for Z And, and $< 2.4 \times 10^{-8} M_{\odot}$ for AG Dra. These authors point out that the Wright and Barlow (1975) formula effectively measures the mass loss associated with the ionized gas only and thus underestimates the true mass-loss rate. They find that even for symbiotic stars with very extended ionized regions, i.e. $X_{H+} > 1$, the Wright-Barlow formula underestimates mass-loss

rates by $\sim 20\%$. For systems with $X_{H^+} < 1$, the mass-loss rate is underestimated by a factor of two or more. We suggest that the Raman efficiencies can be used to provide an independent determination of the X_{H^+} parameter in symbiotic systems providing another useful method by which mass-loss rates of cool giants are examined.

5. O VI Induced Fe II Bowen Fluorescence

Early indirect evidence for the far-UV O VI lines in symbiotic stars included the presence of Fe II transitions ($\lambda 1776.56$, $\lambda 1881.20$, $\lambda 1884.12$) that are selectively photoexcited by the strongest member of the O VI resonance doublet at 1031.9\AA (Johansson 1988). As is the case with the Raman scattered lines in the optical, the Fe II Bowen lines at 1776.56 , 1881.20 , and 1884.12\AA are found in the spectra of symbiotic systems which exhibit other high-excitation lines (Johansson 1988 and Feibelman, Bruhweiler, & Johansson 1991, hereafter FBJ). Weak Fe II Bowen lines have been observed in the IUE spectra of Z And, V1016 Cyg, and RR Tel (Feibelman, Bruhweiler, and Johansson 1991).

We searched for the Fe II Bowen line at 1776\AA in the HUT spectra of our symbiotic stars. One of the lines in the region near the expected location of the Fe II Bowen line is the Si II multiplet near 1814\AA . The ionization potentials of these two species are quite similar and these lines should be formed in roughly the same region. We tied the wavelength of the Fe II Bowen line at 1776\AA to the theoretical wavelength of the $\lambda 1817$ member of the Si II multiplet and fixed the FWHM of the lines to the resolution of the HUT as the Bowen lines are narrow (FBJ).

The Fe II $\lambda 1776$ line is clearly visible in the HUT data for Z And, and is present but extremely weak in V1016 Cyg, and RR Tel, see Figure 5. We did not find evidence for Fe II 1776\AA fluorescent emission in the HUT data for the six remaining systems

(i.e., EG And, BF Cyg, CH Cyg, AG Dra, AX Per, HM Sge) to a 3σ upper limit of 1.0×10^{-13} erg cm $^{-2}$ s $^{-1}$. The non-detections in CH Cyg, AG Dra, and HM Sge are consistent with the IUE results of FBJ, although the authors did report detections of the longer wavelength fluorescent features in HM Sge and AG Dra in the earlier IUE data.

We define the Bowen efficiency, similarly to the Raman efficiency, as the ratio of the number of Fe II $\lambda 1776$ photons to the initially emitted number of O VI $\lambda 1032$ photons. Table 11 lists the extinction corrected fluxes for the Fe II $\lambda 1776.56$ line and the efficiency of the Bowen fluorescence mechanism for each object. The efficiency of the Bowen mechanism is considerably smaller than that for the Raman process, less than 2% in each object. Our derived efficiencies for the production of the Fe II Bowen line at 1776.56\AA are consistent with the efficiencies for the Bowen process in which the C IV $\lambda 1548.2$ line photons photoexcite the Fe II 1975.5\AA line. Simultaneous IUE fluxes for the C IV 1548.2\AA and the Fe II 1975.5\AA lines are reported in FBJ for RR Tel, Z And, and V1016 Cyg and the efficiencies derived from these fluxes are also $< 2\%$ in each object.

6. Summary

From HUT observations and simultaneous or near-simultaneous optical observations we confirm the contemporaneous presence of the O VI $1032, 1038\text{\AA}$ resonance doublet and the Raman scattered O VI emission at $6825, 7082\text{\AA}$ in four of the nine target symbiotic systems, namely Z And, V1016 Cyg, AG Dra, and RR Tel. We calculate scattering efficiencies for each system (Table 9). Our observations show that in no case do we observe the Raman scattered lines in the optical without the simultaneous occurrence of the far-UV O VI emission lines (see Table) thus giving the strongest support to date that the optical emission lines at $6825, 7082\text{\AA}$ are the product of Raman-scattered O VI photons.

The existence of strong O VI and neutral hydrogen in a symbiotic system is a necessary but insufficient condition for the Raman scattering process to occur. Models (Schmid 1996, Harries & Howarth 1997) indicate that the majority of Raman scattered photons are produced in the neutral region between the hot star and the red giant. If the neutral region surrounding the red giant also forms heavy dust condensation, then the far-UV O VI photons may be heavily absorbed and no Raman scattering occurs. This is a strong possibility for HM Sge which has only recently developed Raman lines in the optical (Schmid et al. 2000) and for CH Cyg, which despite evidence for strong O VI emission and significant mass loss from the red giant, does not and apparently never has exhibited the Raman lines. In support of this, both objects have apparently experienced several periods of strong dust condensation around the red giant component (Schmid et al. 2000, Munari et al. 1996).

The Raman scattering efficiency depends strongly on the geometry of the neutral hydrogen scattering region and the mass loss rate (Schmid 1996, Harries & Howarth 1997, Lee & Lee 1997). Schmid has derived efficiencies for various shapes of ionization fronts based on the X_{H^+} -parameterization. For the four systems in which we observed the Raman process, the derived Raman scattering efficiencies imply that X_{H^+} 0.4–4.0, in qualitative agreement with Mürset et al. (1991) and the previously published ORFEUS results (Schmid et al. 1999). The relative mass loss rates of Z And, V1016 Cyg, AG Dra, and RR Tel based on their Raman efficiencies are not in general agreement with those derived from radio measurements (Seaquist et al. 1993). As both the Raman line intensity and polarization profiles are very sensitive to the mass loss rate (Harries & Howarth 1997), detailed studies of these profiles may provide another method to examine mass loss in symbiotic systems.

The presence of Fe II transitions ($\lambda 1776.56$, $\lambda 1881.20$, $\lambda 1884.12$) that are selectively photoexcited by the strongest member of the O VI resonance doublet at 1031.9\AA was

presented as early indirect evidence for the presence of the the far-UV O VI lines at 1032, 1038 Å (Johansson 1988). In our small sample of symbiotic systems, we find no case in which the Fe II 1776.56Å line is present without the simultaneous occurrence of the O VI line at 1032Å. Thus, the HUT data provide the first observational support for the Bowen fluorescence origin of the Fe II 1776.56Å line. Furthermore, the data enable us to make the first estimates of the efficiency for the Bowen fluorescence mechanism responsible for the production of the 1776.56Å in the symbiotic systems Z And, RR Tel, and V1016 Cyg. The derived efficiency is less than 2% in each system.

The prerequisites for the Raman scattering process and the Bowen fluorescence process are quite similar. Both require the presence of strong O VI emission and sufficient amounts of H I and Fe II. Additionally, H I and Fe II have similar ionization potentials, 13.6 eV and 16.2 eV, respectively. Therefore the Raman scattering and Bowen fluorescence processes must both occur in roughly the same region, close to the red giant. Observations from our small sample of symbiotic systems support this: each object which exhibits the Raman scattering process (i.e. Z And, V1016 Cyg, AG Dra, HM Sge, RR Tel) also exhibits some or all of the Fe II Bowen lines (FBJ). CH Cyg shows strong O VI emission but does not exhibit either the Raman lines or the Bowen lines. It might make an interesting study to see if the mutual presence of the Fe II Bowen and Raman lines holds over a larger sample of symbiotics and also if the efficiencies of the two processes are correlated in any way.

The authors wish to thank Drs. Kenyon and Mikołajewska and Drs. Schild & Schmid for providing the optical data for this study. The WIYN data were obtained in a collaboration with Drs. J. Johnson and C. Anderson. We also wish to thank Dr. Dixon for supplying data in advance of publication and Dr. McCandliss for generating the H₂ optical depth templates from the laboratory molecular hydrogen data. We thank the observers of the AFOEV for making their data public and hence aiding in the calibration

of our spectroscopic data. This work was supported by Astro-2 Guest Investigator grant NAG8-1049 to the University of Pittsburgh. Jennifer Birriel acknowledges the support of NASA Graduate Student Researcher Grant NGT5-50174.

REFERENCES

- Abgrall, H., Roueff, E., Launay, F., Roncin, J.-Y., & Subtil, J.-L., 1993a, *A&AS* 101, 273
- Abgrall, H., Roueff, E., Launay, F., Roncin, J.-Y., & Subtil, J.-L., 1993b, *A&AS*, 101, 323
- Allen, D. A. 1980, *MNRAS*, 190, 75.
- Birriel, J. B., Espey, B. R., Schulte-Ladbeck, R. E., 1998, *ApJ*, 507, L75.
- Blair, W. P., Stencel, R. E., Shaviv, G., Feibelman, W. A., 1981, *A&A*, 99, 73.
- Blair, W. P., Stencel, R. E., Feibelman, W. A., Michalitsianos, A. G., 1983, 53, 573.
- Cardelli, J. A., Clayton, G. C., & Mathis, J. S. 1989, *ApJ*, 345, 245.
- Contini, M., Formiggini, L., 1999, *AJ*. 517, 925.
- Dixon, W. Van Dyke, Hurwitz, M., & Bowyer, S., 1998, *ApJ*, 492, 569.
- Espey, B., Keenan, F. P., Mckenna, F. C., Feibelman, W. A., & Aggrawal, K. M., 1996, *ApJ*, 465, 965.
- Espey, B. R., Schulte-Ladbeck, R. E., Kriss, G. E., Hamann, F., Schmid, H. M., Johnson, J. J., 1995a, *ApJ*, 454, L61.
- Espey, B. R., Kriss, G. A., Johnson, J. J., Schulte-Ladbeck, R. E., 1995b *IAUC*, 6148, 2.
- Fernandez-Castro, T., Cassatella, A., Gimenez, A., Viotti, R., 1988, *ApJ*, 324, 1016.
- Fernandez-Castro, T., González-Riestra, R., Cassatella, A., Taylor, A. R., Seaquist, E. R., 1995, *ApJ*, 442, 366.
- Feibelman, W. A., Bruhweiler, F. C., Johansson, S., 1991, *ApJ*, 373, 649. (FBJ)
- Fluks, M. A., Plex, B., The, P. S., De Winter, D., Westerlund, B. E., Steenman, H. C. 1994, *A&AS*, 105, 311.
- González-Riestra, R., Viotti, R., Iijima, T., Greiner, J., 1999, *A&A*, 347, 478.

- Harries, T. J., Howarth, I. D., 1996a, *A&A*, 310, 325.
- Harries, T. J., Howarth, I. D., 1996b, *A&AS*, 119, 61.
- Harries, T. J., Howarth, I. D., 1997, *A&AS*, 121, 15.
- Hayes, D., Latham, D. W., 1975, *ApJ*, 197, 593.
- Hric, L., Skopal, A., Urban, Z., Petřík, K., Komžík, R., Chochol, D., Pribulla, T., Niarchos, P., Rovithis-Livaniou, H., Rovithis, P., Kaserkevich, V.S., Shpychka, I.V., Velič, Z., Halevin, A.V., Andronov, I.L., Okša, G. and Krtička, J. 1996, *Contrib. Astron. Obs. Skalnaté Pleso*, **26**, 46.
- Hric, L., Skopal, A., Urban, Z., Petřík, K., Komžík, R., Chochol, D., Pribulla, T., Niarchos, P., Rovithis-Livaniou, H., Rovithis, P., Kaserkevich, V.S., Shpychka, I.V., Velič, Z., Halevin, A.V., Andronov, I.L., Okša, G. and Krtička, J. 1996, *Contrib. Astron. Obs. Skalnaté Pleso*, **27**, 121
- Iverson, R. J., Bode, M. F. & Meaburn, J., 1994, *A&AS* 103, 201.
- Johansson, S., 1988, *ApJ*, 327, L85.
- Kenyon, S. J., Webbink, R. F., 1984, *ApJ*, 279, 252.
- Kenyon, S. J., Fernandez-Castro, T., 1987, *AJ*, 93, 938.
- Kriss, G. A. 1994, in *ASP Conf. Proc. 61, Astronomical Data Analysis Software and Systems III*, ed. D.R. Crabtree, R.J. Hanisch, & J. V. Barnes, (San Francisco: ASP), 437.
- Kruk, J. W., Durrance, S. T., Kriss, G. A., Davidsen, A. F., Blair, W. P., Espey, B. R. 1995, *ApJ*, 454, L1.
- Kruk, J. W., Kimble, R. A., Buss, R. H., Davidsen, A. F., Durrance, S. T., Finley, D. S., Holberg, J. B., Kriss, G. A., 1998 *ApJ* in press.

- Kruk, J.W., Brown, T.M., Davidsen, A.F., Espey, B.R., Finley, D.S. and Kriss, G.A. 1999
ApJS 122, 299.
- Lee, K. W., Lee, H.-W., 1997a, MNRAS, 287, 211.
- Lee, K. W., Lee, H.-W., 1997b, MNRAS, 292, 573.
- Li, P. S., Leahy, D. A., 1997, ApJ, 484, 424.
- Mikołajewska, J., Selvelli, P. L., Hack, M., 1988 A&A, 198, 150.
- Mikołajewska, J., Kenyon, S. J., Mikołajewska, M., 1989, ApJ, 98, 1427.
- Mikołajewska, M., Mikołajewska, J., Khudyakova, T. N., 1990 A&A, 235, 219.
- Mikołajewska, J., & Kenyon, S. J., 1992, AJ, 103, 579.
- Mikołajewska, J., Kenyon, S. J., Mikołajewska, M., Garcia, M. R., Polidan, R. S., 1995, AJ, 109,
1289.
- Mikołajewska, J., & Kenyon, S. J., 1996, AJ, 112, 1659.
- Morton, D. C. 1975, ApJ, 197, 85.
- Morton, D. C. 1991, ApJS, 77, 119.
- Munari, U., Yudin, B. F., Kolotilov, E. A., Tomov, T. V., 1996, A&A, 311, 484.
- Mürset, H., Nussbaumer, H., Schmid, H. M., Vogel, M. 1991, A&A, 248, 458.
- Nussbaumer, H., Schild, H., 1981, ApJ, 101, 118.
- Nussbaumer, H., & Storey, P. J. 1984, A&AS, 56, 293.
- Nussbaumer, H., Schmid, H. M., Vogel, M., 1989 A&A, 211, L27.
- Nussbaumer, H., Vogel, M., 1990, A&A, 236, 117.
- Nussbaumer, H., Dumm, T., 1997, A&A, 323, 387.
- Pacheco, J. A. De Freitas, Codina-Landaberry, S. J., Lopes, D. F., 1989, ApJ, 337, 520.

- Penston, M. V., Benvenuti, P., Cassatella, A., Heck, A., Selvelli, P., 1983, MNRAS, 202, 833.
- Proga, D., Mikolajewska, J., Kenyon, S. J., 1994, MNRAS, 268, 213.
- Proga, D., Kenyon, S. J., Raymond, J. C., 1996, ApJ, 471, 930.
- Schlegel, D., Finkbeiner, D., Davis, M., 1998 ApJ 500, 525. (SFD)
- Schmid, H. M., 1989, A&A, 211, L31.
- Schmid, H. M., 1992, A&A, 254, 224.
- Schmid, H. M., 1996, MNRAS, 282, 511.
- Schmid, H. M., Schild, H., 1990, MNRAS, 246, 84.
- Schmid, H. M., Schild, H., 1994, A&A, 281, 145.
- Schmid, H. M., Schild H. 1997a, A&A, 321, 791.
- Schmid, H. M., Schild H. 1997b, A&A, 327, 219.
- Schmid, H. M., Krautter, J., Appenzeller, I., Barnstedt, J., Dumm, T., Gölz, M., Grewing, M., Gringel, W., Haas, C., Hopfensitz, W., Kappelmann, N., Krämer, G., Lindenberger, A., Mandel, H., Mürset, U., Schild, H., Schmutz, W., Widmann, H., 1999, A&A, 348, 950.
- Schmid, H. M., Corradi, R., Krautter, J., Schild, H., 2000, A&A, 365, 261.
- Seaquist, E. R., Krogulec, M., Taylor, A. R., 1993, ApJ, 410, 260.
- Seaquist, E. R., Taylor, A. R., Button, S. 1984, ApJ, 284, 202; erratum: ApJ, 317, 555.
- Storey, P. J., Hummer, D. G., 1995, MNRAS, 272, 41.
- Tomova, M. T., Tomov, N. A., 1999, A&A, 347, 151.
- van Dishoeck, E. F., & Black, J. H., 1986, ApJS, 62, 109.

Wright, A. E., Barlow, M. J., 1975, MNRAS, 170, 41.

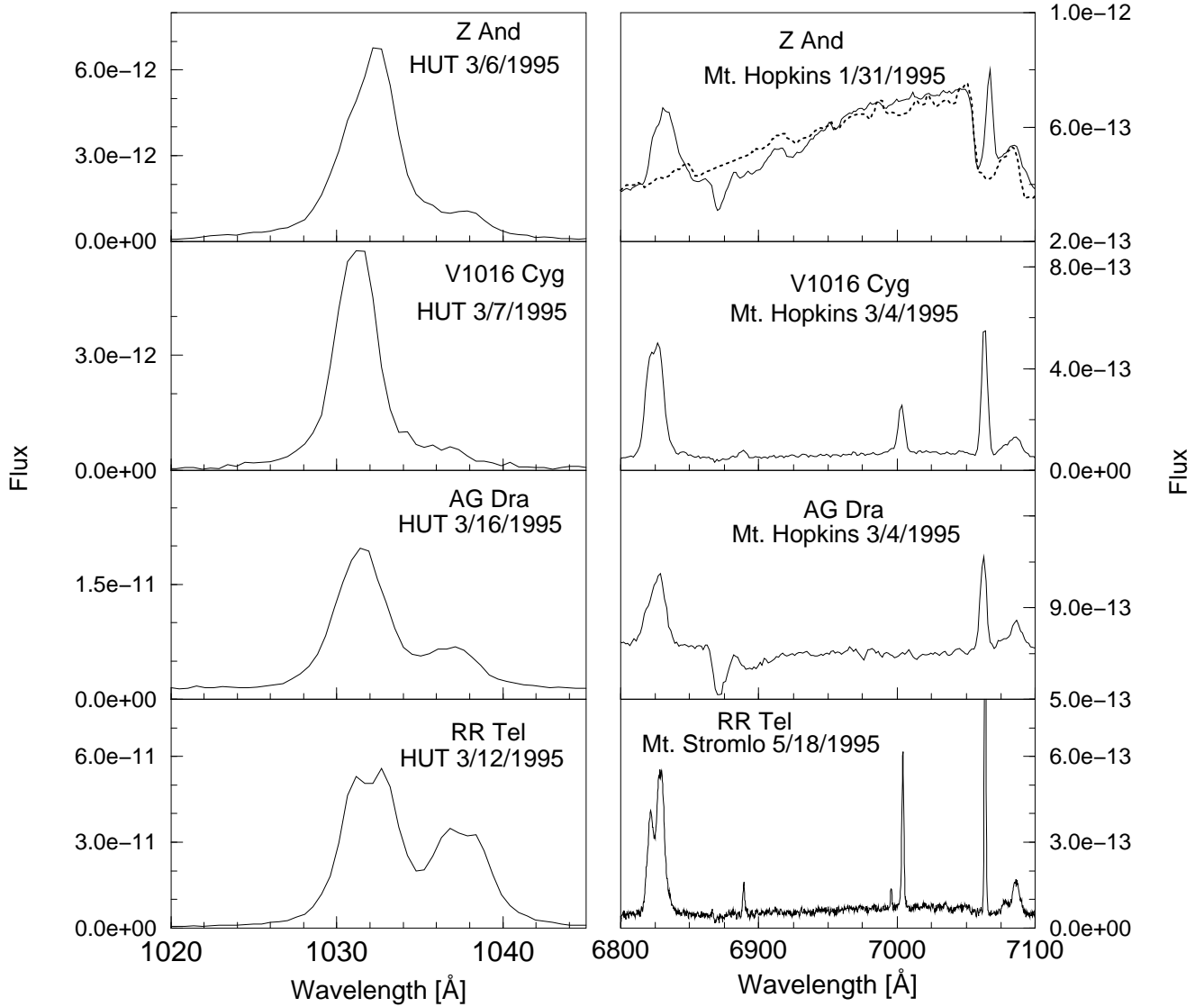


Fig. 1.— HUT far-UV and ground-based optical data for objects exhibiting both the direct and Raman scattered O VI lines. Fluxes are in units of $\text{ergs cm}^{-2} \text{s}^{-1} \text{Å}^{-1}$. Dotted lines represent our fits to the continuum of the M giant star.

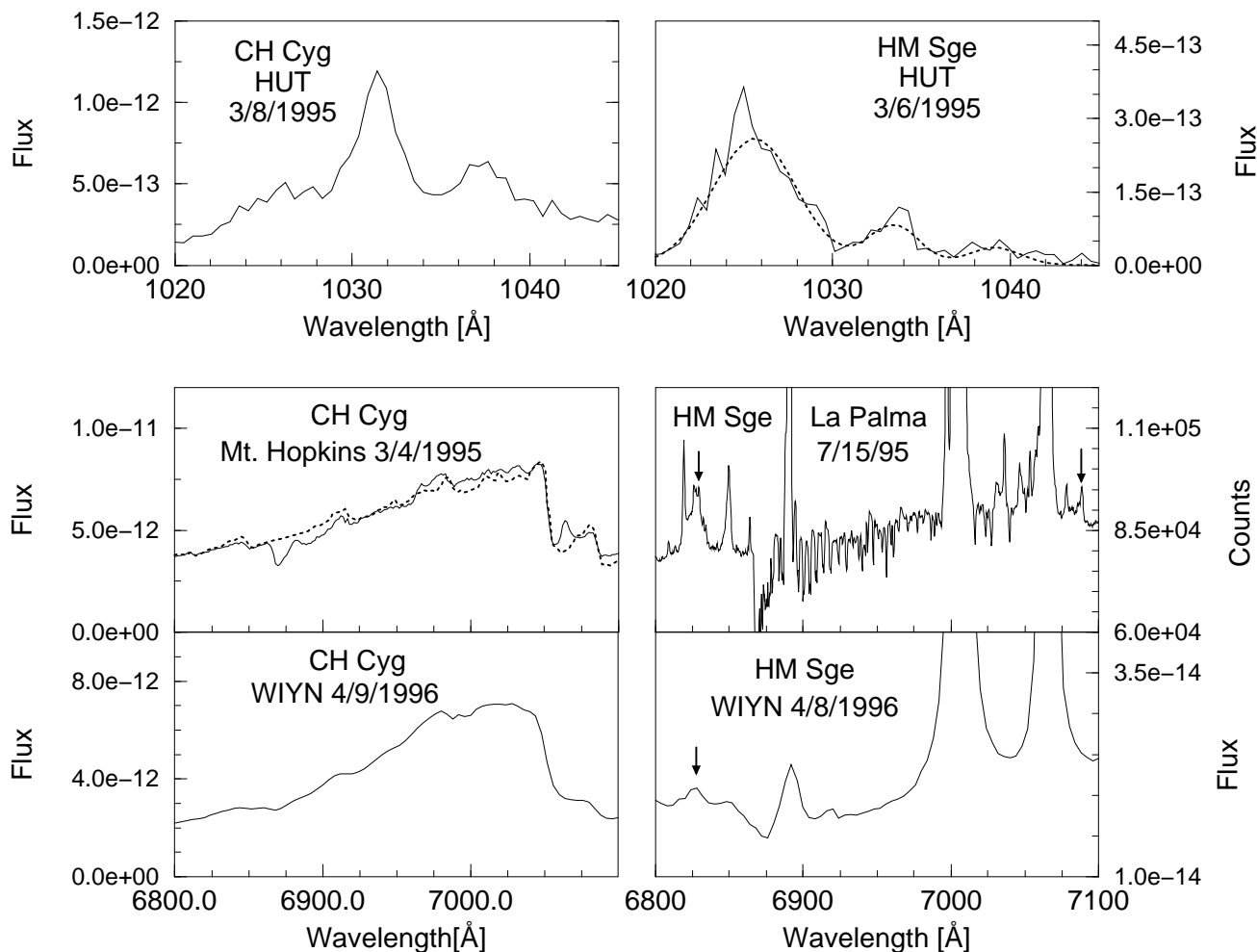


Fig. 2.— HUT and optical data for objects showing direct O VI lines in the far-UV and no Raman lines or extremely weak Raman lines (indicated by arrows) in the optical. Fluxes are in units of $\text{ergs cm}^{-2} \text{s}^{-1} \text{\AA}^{-1}$. The emission feature near $\lambda 1026\text{\AA}$ in the spectrum of HM Sge is terrestrial Ly β airglow and the dotted lines represent our best fit to the Ly β and the weak O VI lines.

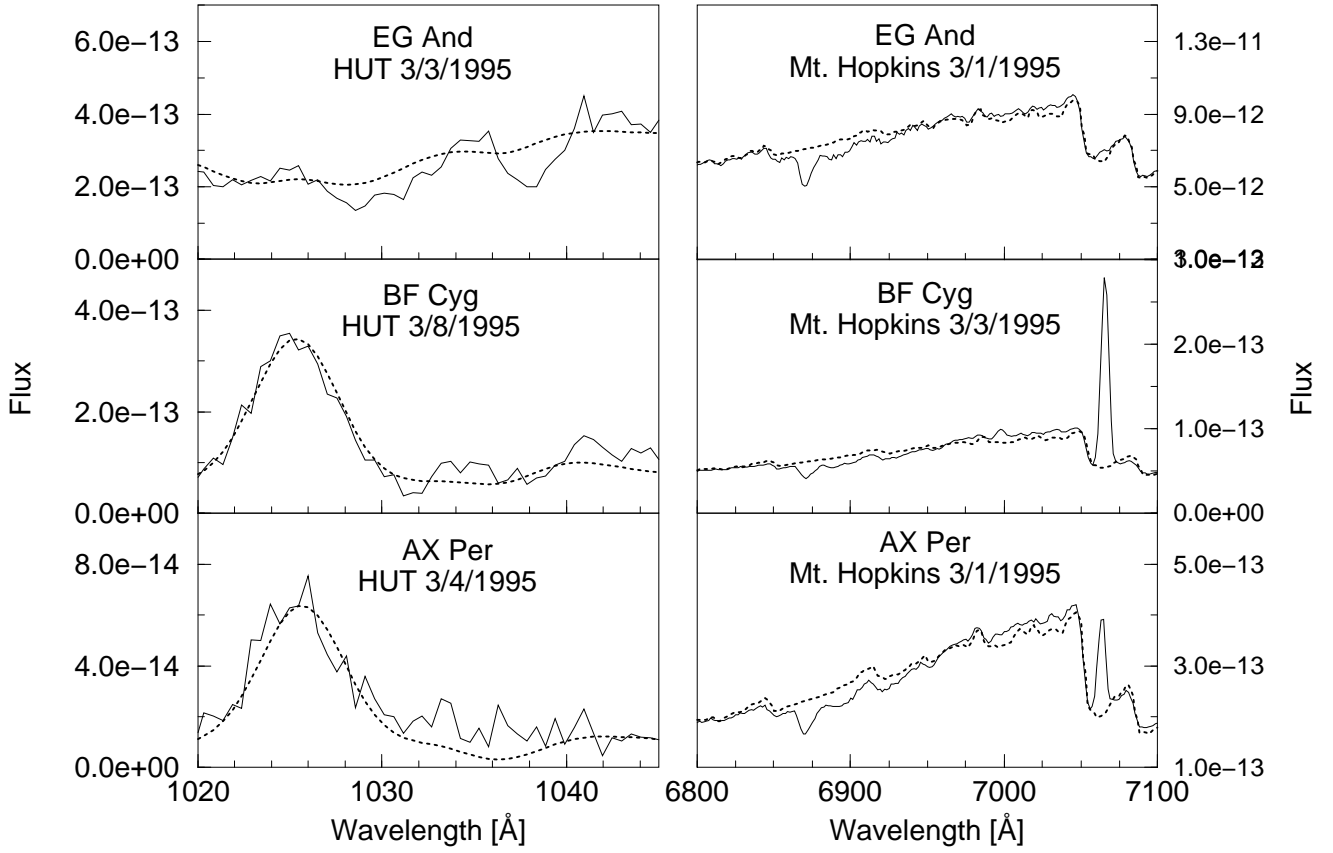


Fig. 3.— HUT and optical data for objects showing neither the far-UV O VI lines nor the optical emission. Fluxes are in units of $\text{ergs cm}^{-2} \text{s}^{-1} \text{\AA}^{-1}$. The emission feature near $\lambda 1026\text{\AA}$ in the spectra of BF Cyg and AX Per is terrestrial Ly β airglow. Dotted lines represent our fits to the continuum.

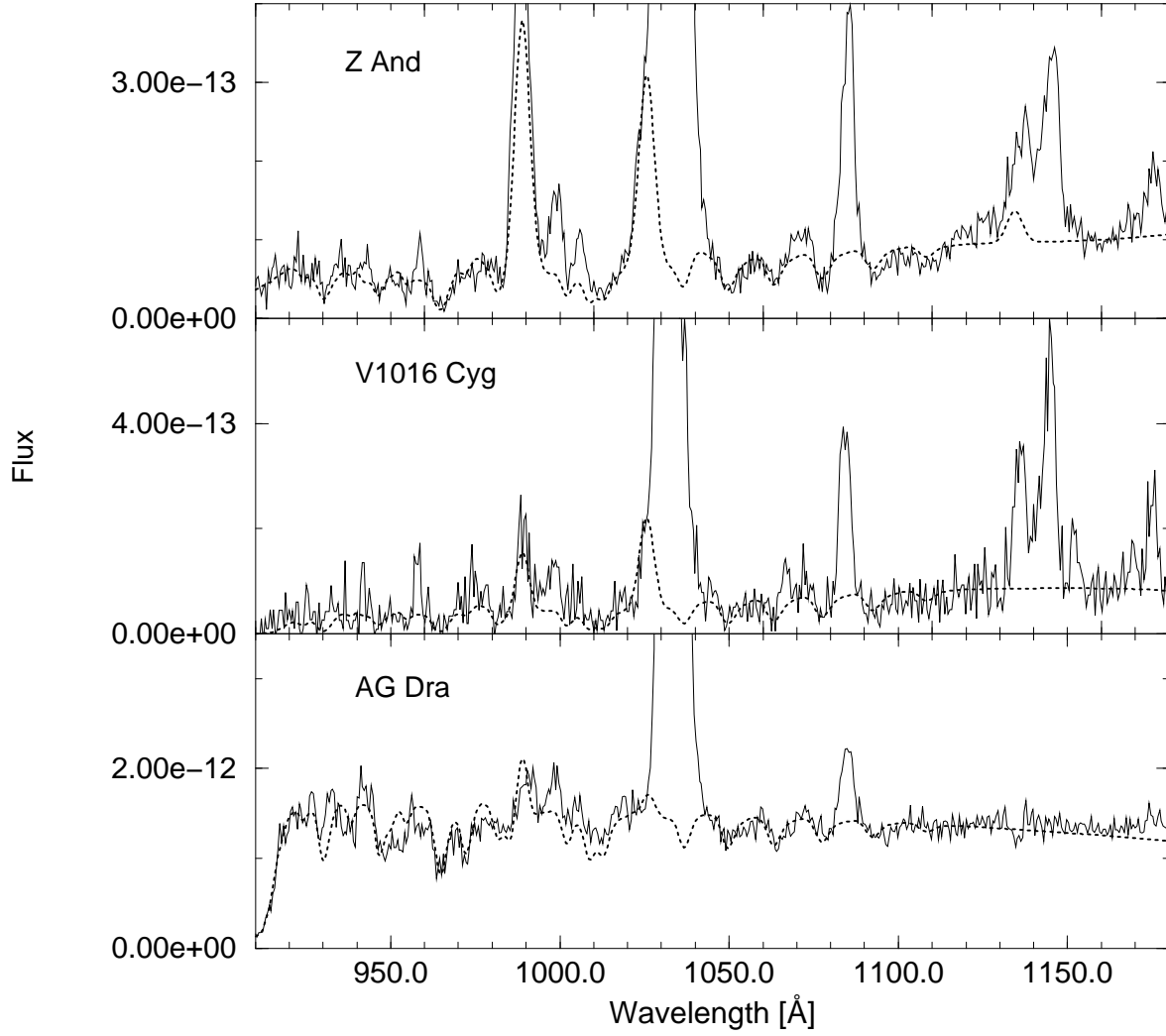


Fig. 4.— Far-UV continuum fits for Z And, V1016 Cyg, and AG Dra. The fits (dotted lines) consist of a blackbody spectrum reddened with the extinction curve of CCM (1989) and absorbed by interstellar H I and H₂. In addition, we included terrestrial airglow from N I (weakly visible at λ 913Å), O I (989Å), and H I (λ 939 Å, λ 950Å, 973Å, λ 1026Å). Fluxes are in units of $\text{ergs cm}^{-2} \text{s}^{-1} \text{Å}^{-1}$.

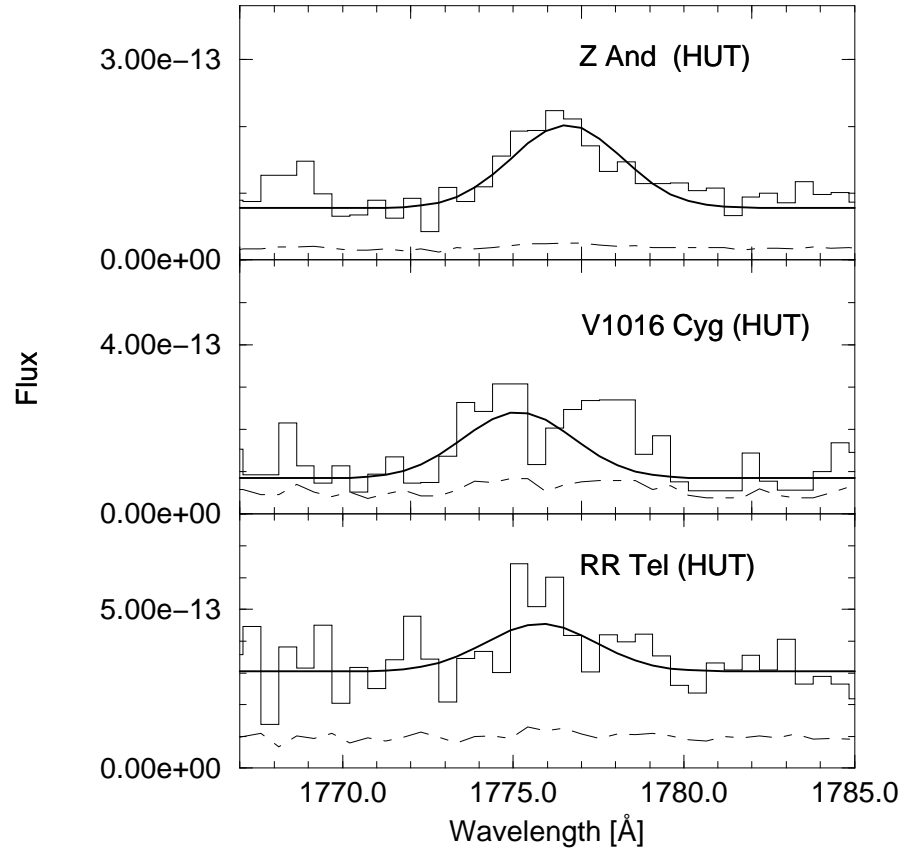


Fig. 5.— HUT data showing the weak Fe II Bowen Fluorescence lines at λ 1776. Fluxes are in units of $\text{ergs cm}^{-2} \text{s}^{-1} \text{\AA}^{-1}$. The thick solid lines show our best fit to the data. The thick dot-dash line is the error array for the data.

Table 1a
HUT Far UV Spectra

Target	Start Time ^a (UT)	Exposure (s)	Door (cm ²)	Slit Diameter (arcsec)	Photometric Correction	S/N Near O VI Lines
EG And	Mar 15 06:29:55	1328	5120	20	1.0343	10
Z And	Mar 6 01:21:44	1370	5120	20	1.0091	10
BF Cyg	Mar 8 03:37:02	796	5120	20	1.2287	8
CH Cyg	Mar 13 02:39:55	1082	5120	20	1.0993	10
V1016 Cyg	Mar 6 23:58:58	664	2560	12	1.6483	4
AG Dra	Mar 16 19:14:18	764	2560	20	1.0057	15
AX Per	Mar 4 02:15:59	548	5120	20	1.5631	4
HM Sge	Mar 6 10:24:34	1026	5120	20	1.0817	1
RR Tel	Mar 12 14:21:53	994	750	20	1.0167	10

^aAll observations obtained during orbital day.

Table 1b

Optical Spectra

Target	Date	Telescope ^a	Photometric Scale Factor ^b	Reference
EG And	Jan 3 1995	Mt. Hopkins	1.70	Mikołajewska & Kenyon (1996) (MK)
Z And	Jan 31 1995	Mt. Hopkins		MK
BF Cyg	Mar 3 1995	Mt. Hopkins		MK
CH Cyg	Apr 3 1995	Mt. Hopkins		MK
	Apr 9 1996	WIYN		
V1016 Cyg	Apr 3 1995	Mt. Hopkins		MK
AG Dra	Apr 3 1995	Mt. Hopkins	5.10	MK
AX Per	Jan 3 1995	Mt. Hopkins	2.36	MK
HM Sge	Jul 15 1995	La Palma		Schmid & Schild 1997b
	Apr 8 1996	WIYN		
RR Tel	May 18 1995	Mt. Stromlo		Espey et al. 1995a

^aMt. Hopkins Observatory 1.5m telescope; La Palma Observatory 4.2m telescope; WIYN: Wisconsin Indiana Yale NAO 3.5m telescope; Mt. Stromlo Observatory 1.88m telescope

^bFor observations affected by clouds, see §2.

Table 2
 Observed Fluxes ($\text{erg cm}^{-2} \text{s}^{-1}$) of Direct &
 Raman Scattered O VI Lines in Selected Symbiotic Stars

Object	O VI ^a		Raman Scattered	
	1032	1038	6825	7082
EG And	< 3.0E-14	< 2.0E-14	< 6.0E-14	< 1.5E-13
Z And	2.6E-11	4.2E-12	4.2E-12	1.3E-12
BF Cyg	< 1.5E-14	< 1.5E-14	< 1.1E-15	< 2.5E-15
CH Cyg	3.1E-12	1.6E-12	< 4.0E-14	< 1.0E-14
V1016 Cyg	1.9E-11	2.1E-12	6.6E-12	1.1E-12
AG Dra	7.1E-11	2.2E-11	4.5E-12	1.9E-12
AX Per	< 5.1E-14	< 5.4E-14	< 1.3E-15	< 1.9E-14
HM Sge ^b	3.1E-13	1.4E-13	3.7E-14	<5.1E-14
RR Tel	2.3E-10	1.4E-10	5.4E-12	1.0E-12

^aO VI lines measured relative to a local linear continuum.

^bWIYN observation on 8 April 1996.

Note. — Where lines are absent, we give the 3σ upper limit on fluxes. UV line fluxes are accurate to $\sim 6\%$. Optical line fluxes good to $\sim 10\%$.

Table 3
Hot Star Zanstra Temperatures.

Object	T_{WD} (K) ^a	
	This Work	Mürset et al. 1991
EG And	76,000	80,000 (Nov. 1990)
Z And	110,000	130,000 (Nov. 1987)
BF Cyg	64,000	55,000 (July 1986)
CH Cyg	58,000 ^b	80,000 (Nov. 1988)
V1016 Cyg	135,000	145,000K (Nov. 1987)
AG Dra	86,000 ^b	125,000 (June 1985)
AX Per	89,000	105,000 (Oct. 1984)
HM Sge	165,000	200,000 (Oct. 1990)
RR Tel	130,000	140,000 (June 1983)

^aUncertainties of $\pm 20\%$

^bOutburst, see text.

Table 4

Extinction values from the literature.

Object	E(B-V)	Method	Reference
EG And	0.10±0.01	UV continuum fit	this work
	0.09±0.01	Dust maps	SFD ^a (1998)
	0.05	Shape of UV continuum	Mürset et al. (1991)
Z And	0.24±0.03	He II 1640/4686, 1085/4686	Birriel et al. (1998)
	0.21±0.01	UV continuum fit	this work
	0.21±0.03	Dust maps	SFD (1998)
	0.30	2200Å feature	Mürset et al. (1991)
	0.2-0.3	H I Balmer lines	Mikołajewska & Kenyon (1996)
BF Cyg	0.24±0.01	UV continuum fit	this work
	0.29±0.05	Dust maps	SFD (1998)
	0.35	2200Å feature	Mürset et al. (1991)
	0.40±0.05	UV continuum fit	Mikołajewska et al. (1989)
CH Cyg	0.08±0.01	Dust maps	SFD 1998
	0.10	Shape of UV continuum	Mürset et al. (1991)
	0.00	absence of 2200Å feature	Mikołajewska et al. (1988)
V1016 Cyg	0.24±0.03	UV continuum fit	this work
	0.35±0.04	He II 1640/4686, 1085/4686	this work
	0.25±0.04	Dust maps	SFD (1998)
	0.40	2200Å feature	Mürset et al. (1991)
	0.17±0.02	UV continuum fit	Kenyon & Webbink (1984)
	0.20±0.10	[Ne V] 1575/2973 ratio	Nussbaumer & Schild (1981)
	0.28	2200Å feature	Nussbaumer & Schild (1981)

Table 4, cont.'d

Extinction values from the literature.			
Object	E(B-V)	Method	Reference
AG Dra	0.08±0.01	UV continuum fit	this work
	0.07±0.01	He II 1640/4686	this work
	0.12±0.02	He II 1085/4686	this work
	0.15±0.02	He II 1085/1640	this work
	0.11±0.01	Dust maps	SFD (1998)
	0.00	Shape of UV continuum	Mürset et al. (1991)
	0.06±0.01	He II 1640/4686	Mikołajewska et al. (1995)
	0.05±0.01	UV continuum fit	Mikołajewska et al. (1995)
AX Per	0.25±0.03	UV continuum fit	this work
	0.22±0.03	Dust maps	SFD (1998)
	0.32±0.02	He II 1640/4686	Mikołajewska & Kenyon (1992)
	0.25	2200Å feature	Mürset et al. (1991)
	0.28	H I Balmer lines	Blair et al. (1983)
HM Sge	0.65±0.10	Dust maps	SFD (1998)
	0.65	2200Å feature	Mürset et al. (1991)
	0.56±0.14	H I Balmer lines	Pacheco et al. (1989)
	0.40	H I Balmer lines	Blair et al. (1981)
RR Tel	0.08±0.02	Ne V 1575/2973	Espey et al. (1996), this work
	0.05±0.01	Dust maps	SFD (1998)
	0.10	Shape of UV continuum	Mürset et al. (1991)
	0.10	He II recombination lines	Penston et al. (1983)

Note. — Adopted extinctions appear in bold.

^aSchlegel, Finkbeiner, & Davis.

Table 5

Optical Spectral Types for Cool Components

Object	This Study/Orbital Phase	Kenyon & Fernandez-Castro 1987
EG And	M2.9±0.5 III/0.99	M2.4±0.3 III
Z And	M4.1±0.5 III/0.33	M3.5±1 III
BF Cyg	M4.2±0.5 III/0.88	M5±1 III
CH Cyg	M5.0±0.5 III/0.62	M6.5±0.3 III
AX Per	M4.7±0.5 III/0.17	M5.2±0.4 III

Table 6

Model Continuum Parameters

Object	T _{WD} ^a	T _{Neb} ^b	E(B-V)	log N(HI)	log N(H ₂)
Z And	110,000K	20,000 K	0.21±0.01	21.30±0.08	20.06±0.05
V1016Cyg	135,000	10,000 K	0.24±0.03	21.79±0.82	20.27±0.07
AG Dra	125,000	15,000 K	0.08±0.01	20.80±0.26	19.70±0.04

^aBlackbody temperature of white dwarf, fixed, see text.

^bNebular electron temperature; fixed, see text.

Table 7

H ₂ Absorption Correction Factors					
Object	log N(H ₂)	O VI Line Width ^a	V _{Rad} ^b	Transmission Coefficient	
		(km s ⁻¹)	(km s ⁻¹)	1031.928	1037.617
Z And	20.06±0.05	70	12	0.976±0.003	0.381±0.042
V1016Cyg	20.27±0.07	70	-52	0.961±0.006	0.248±0.049
AG Dra	19.70±0.04	70	-138	0.977±0.002	0.618±0.023

Note. — The relative velocity of the absorbing H₂ cloud and the symbiotic system is assumed to be $0.5|V_{Rad}|$, see text.

^aSchmid et al. 1998

^bHeliocentric radial velocity of object ± 4 km s⁻¹ (Ivison, Bode, Meaburn 1994).

Table 8

O VI line fluxes (in 10 ⁻¹² erg cm ⁻² s ⁻¹) relative to H ₂ Absorbed Continuum							
Object	Observed			E(B-V) (mag)	Corrected ^a		
	1032	1038	$\frac{F(1032)}{F(1038)}$		1032	1038	$\frac{F(1032)}{F(1038)}$
Z And	26±1	4.1±0.2	6.3	0.24±0.03	730±300	280±120	2.6
V1016Cyg	19±1	2.1±0.2	9.0	0.24±0.03	550±220	220±100	2.5
AG Dra	70±3	23±1	3.0	0.08±0.02	220±30	100±15	2.2

^aAbsorption and extinction corrected. Quoted error includes uncertainty in absorption and extinction.

Table 9
 O VI Line Flux Variations
 Observed Flux in (10^{-12} erg cm $^{-2}$ s $^{-1}$)^a / Orbital Phase

	1993 ^b	1995	1996 ^b
Z And			
1032Å	25±1 / 0.67	26±1 / 0.39	35 $^{+7}_{-4}$ / 0.21
1038Å	2.5±0.3 / 0.67	4.2±0.2 / 0.39	4.2 $^{+0.8}_{-0.4}$ / 0.21
V1016 Cyg			
1032Å	NA ^c	19±1	19±1
1038Å	NA ^c	2.1±0.1	1.0±0.1
AG Dra			
1032Å	95±5 / 0.18	72±4 / 0.66	62 $^{+12}_{-6}$ / 0.28
1038Å	42±4 / 0.18	23±1 / 0.66	21 $^{+4}_{-2}$ / 0.28
RR Tel			
1032Å	256±5	232±11	218±22 ^d
1038Å	154±5	143±7	132±13 ^d

^aMeasured relative to a local linear continuum.

^bOrfeus-I and -II, Schmid et al. 1999

^cNo spectrum available.

^d21 Nov 1996 Echelle spectrum observation.

Table 10

Raman Scattering Efficiencies

Extinction corrected O VI and Raman line fluxes in ($10^{-12}\text{erg cm}^{-2} \text{ s}^{-1}$)

Raman efficiency is the ratio of observed Raman photons to *initial* number of O VI photons.

Object	O VI ^a		Raman		N _{Raman} /N _{O VI} (%)	
	1032	1038	6825	7082	N ₆₈₂₅ /N ₁₀₃₂	N ₇₀₈₂ /N ₁₀₃₈
Z And	730±300	280±120	7.3±0.9	2.2±0.5	7±3	5±2
V1016 Cyg	550±220	220±100	14.4±2.0	2.2±0.3	15±6	6±3
AG Dra	220±30	100±15	5.4±0.6	2.2±0.2	14±2	13±2
RR Tel	700±190	430±120	6.7±1.0	1.3±0.3	6.0±1.9	2.0±0.7

^aIncludes corrections for H₂ absorptions, see Table 7.

Table 11

Bowen Fluorescence Efficiencies

Extinction corrected O VI and Fe II Bowen line fluxes in units of

$10^{-13}\text{erg cm}^{-2} \text{ s}^{-1}$. The photon ratio N_{FeII}/N_{O VI}

is the Bowen fluorescence efficiency.

Object	F(O VI λ 1032)	F(Fe II λ 1776)	N ₁₇₇₆ /N ₁₀₃₂
Z And	7300±300	24±6	(0.6±0.3)%
V1016 Cyg	5500±2200	56±18	(1.7±0.9)%
RR Tel	7000±1900	10.8±3.0	(0.3±0.1)%